J Math Chem (2014) 52:1338–1349
DOI 10.1007/s10910-014-0313-5

ORIGINAL PAPER

Exact steady state solutions in symmetrical Nernst–Planck–Poisson electrodiffusive models

Andrey V. Shobukhov · **Dmitry S. Maximov**

Received: 2 August 2013 / Accepted: 22 January 2014 / Published online: 2 February 2014

Abstract We compare three one-dimensional Nernst–Planck–Poisson systems that describe ion distribution near the electrode surfaces with planar, cylindrical and spherical symmetry respectively. These three models take into account ion diffusion and migration. In particular they describe the diffusive layers formed by Li+ ions in the vicinity of the graphite electrode particles. The three types of symmetry appear due to three different ways of particle ordering inside the electrode. In this paper we construct the exact steady state solutions to these systems and approximate solutions in form of power series. Then we solve the systems numerically and compare the results. We discuss the influence of symmetry in electrode particle ordering on the steady state distribution of ions in the diffusive layer.

Keywords Nernst–Planck–Poisson system · Exact steady state solutions · Electrodiffusion · Symmetry

Mathematics Subject Classification 35K51 · 65C20 · 65N06 · 78A57

1 Introduction

The porous electrodes are loosely formed of separate particles that accumulate the ions from the surrounding electrolyte. In particular, intercalation and deintercalation of Li+

A. V. Shobukhov (✉)
Lab for Mathematical Modeling in Physics, Faculty of Computational Mathematics and Cybernetics, Lomonosov Moscow State University, Moscow 119991, Russia
e-mail: shobukhov@cs.msu.su

D. S. Maximov
Moscow Radiotechnical Institute of the Russian Academy of Sciences, Varshavskoye Shosse, 132, Moscow 117519, Russia

ions into and out of carbon particles make the basis of the Li-ion battery functioning [1–5]. Significantly less attention is paid to the distribution of ions in the diffusive layers adjacent to the particle surfaces. Meanwhile the formation of ion congestions around the particles is the important prerequisite for further intercalation [6–10].

Ion density inside the porous electrode strongly depends on the electrode structure. It is well established experimentally that the particles may form carbon films, carbon fibers or shapeless carbon clods inside the electrode [5,10]. These three cases correspond to the flat, cylindrical and spherical symmetry; consequently we obtain three single particle models [5–7,12] for the description of ion diffusion and migration: the origin is placed at a randomly chosen single particle and it becomes a representative of all other electrode particles; then the Nernst–Planck–Poisson system [11–14] in Cartesian, cylindrical or spherical coordinate system is written down with respect to this origin. Unlike [15], in this paper we do not study intercalation at the surface of the particle itself, but are interested in the dynamics of ion concentration and electric potential around it.

Following [13], in this paper we assume that in all three cases our models are symmetric with respect to two spatial coordinates out of three and thus are one-dimensional. We construct the exact steady state solutions for our models and compare the final ion concentrations and electrical potentials obtained in different geometries for the same parameter values. Then we study numerically the evolution of the initial ion distributions in the neighborhood of an electrode particle. Such wise we evaluate the influence of the electrode structure on the rate of the processes inside it.

2 Mathematical model

Let us consider three one-dimensional variants of the single particle model. If all particles belong to the same plane, then the only significant spatial variable is the one perpendicular to this plane; we obtain the Cartesian 1D model. If all particles lie on the same line then the coordinate along this line and the angular coordinate are insufficient, and the only significant spatial variable is the radius in the plane perpendicular to this line; it gives us the cylindrical 1D model. Finally, if the particles are not ordered at all and make a carbon clod, then the only significant spatial variable is the distance from the origin (the length of the radius vector); this case yields the spherical 1D model.

Let θ be the normalized concentration of the Li+ ions ($0 \leq \theta \leq 1$) and let φ be the electric potential. Then the electrodiffusive processes inside electrolyte in the single particle neighborhood are described by the Nernst–Planck–Poisson system of equations:

$$\frac{\partial \theta}{\partial t} = D \cdot div \left(grad\, \theta + \frac{z \cdot F}{RT} \cdot \theta \cdot grad\, \varphi \right), \tag{1}$$

$$div\, grad\, \varphi = -\frac{4\pi \cdot F}{\varepsilon} \cdot C_{\max} \cdot \theta. \tag{2}$$

Here z = +1 is the electrical charge of the Li+ ion, D is the diffusion coefficient of these ions in the electrolyte, ε is the electrical permittivity of media and C_{max} is

the maximal possible concentration of the Li+ ions in it. The system (1)–(2) may be rewritten for the considered symmetrical 1D models in the following way:

$$\frac{\partial\theta}{\partial t} = D \cdot div\left(grad\,\theta + \frac{z \cdot F}{RT} \cdot \theta \cdot grad\,\varphi\right); \tag{3}$$

$$\frac{1}{r^n} \cdot \frac{\partial}{\partial r}\left[r^n \cdot \frac{\partial\varphi}{\partial r}\right] = -\beta \cdot \theta, \tag{4}$$

$$\alpha = \frac{zF}{RT}, \quad \beta = \frac{4\pi F}{\varepsilon} \cdot C_{\max}, \quad n = 0, 1, 2; \quad 0 < r < R_{\max}, \quad 0 < t < T_{\max}.$$

Here n = 0, 1 and 2 stands for the Cartesian, cylindrical and spherical cases respectively. The spatial coordinate r belongs to the interval $(0; R_{max})$. We consider two sets of boundary conditions for (3)–(4):

$$\frac{\partial\theta}{\partial r} = 0, \quad \frac{\partial\varphi}{\partial r} = 0 \quad at\ r = 0; \tag{5}$$

$$\theta = \theta^*, \quad \varphi = \varphi^* \quad at\ r = R_{\max}, \tag{6}$$

The boundary conditions (6) mean the absence of gradients of the electric potential and the diffusive ion flux at r = 0, and that both the ion concentration and the electric potential remains constant at $r = R_{max}$. The initial conditions for (3)–(4)

$$\theta(0, r) = f(r), \quad \varphi(0, r) = 0. \tag{7}$$

imply that initially no potential is applied and the ions are distributed according to the given law f = f(r).

The existence and the asymptotes of the weak solutions to (3)–(7), as well as the appropriate numerical methods were studied in details in [11–13] and particularly in [14], but very few results have been obtained for the classical solutions to this problem.

3 Steady state solutions

3.1 Power series solution

Let $\theta = \theta(r)$ and $\phi = \phi(r)$ be the steady state solutions to (3)–(6). Then they satisfy the system:

$$\frac{d}{dr}\left[r^n \cdot \left(\frac{d\theta}{dr} + \alpha \cdot \theta \cdot \frac{d\varphi}{dr}\right)\right] = 0, \tag{8}$$

$$\frac{1}{r^n} \cdot \frac{d}{dr}\left[r^n \cdot \frac{d\varphi}{dr}\right] = -\beta \cdot \theta, \tag{9}$$

$$\frac{d\theta}{dr} = 0, \quad \frac{d\varphi}{dr} = 0 \quad at\ r = 0; \tag{10}$$

$$\theta = \theta^*, \quad \varphi = \varphi^* \quad at\ r = R_{\max}. \tag{11}$$

Following [12], we introduce the function s = s(r):

$$s(r) = \int_0^r \theta(\rho) \cdot \rho^n d\rho,\ n = 0, 1, 2; \quad therefore \quad \frac{ds}{dr}(r) = \theta(r) \cdot r;$$
$$\frac{d^2 s}{dr^2}(r) = \frac{d\theta}{dr}(r) \cdot r + \theta(r). \tag{12}$$

We integrate (8) and (9) from 0 to r, take into account the boundary conditions (10) and obtain:

$$\frac{d\theta}{dr}(r) + \alpha \cdot \theta(r) \cdot \frac{d\varphi}{dr}(r) = 0; \quad r^n \frac{d\varphi}{dr}(r) = -\beta \cdot s(r). \tag{13}$$

The final yield of expressions (12) and (13) is the second order equation with respect to s = s(r):

$$\frac{d^2 s}{dr^2} = \frac{1}{r^n} \cdot \frac{ds}{dr}(r) \cdot [\kappa(n) + \alpha \cdot \beta \cdot s(r)], \quad where\ \kappa(n) = \begin{cases} 0\ for\ n = 0 \\ 1\ for\ n = 1 \\ 2r\ for\ n = 2 \end{cases}. \tag{14}$$

We seek the solution to (14) in form of power series with respect to r:

$$s(r) = s_0 + s_1 \cdot r + s_2 \cdot r^2 + s_3 \cdot r^3 + \cdots. \tag{15}$$

We introduce the new parameter: $\sigma = d^{n+1}s/dr^{n+1}(0)$. Now the conditions for (15) at r = 0 look as follows:

$$\begin{array}{l} s(0) = 0, \quad ds/dr(0) = \sigma \quad for\ n = 0; \\ s(0) = 0, \quad ds/dr(0) = 0, \quad d^2 s/dr^2(0) = \sigma \quad for\ n = 1; \\ s(0) = 0, \quad ds/dr(0) = 0, \quad d^2 s/dr^2(0) = 0, \quad d^3 s/dr^3(0) = \sigma \quad for\ n = 2. \end{array} \tag{16}$$

We substitute (15) and its formal derivatives into (14), take into account (16) and equate the coefficients at the equal powers of r. We obtain the infinite recurrent system of equations for s_k, which yields:

Using (12), we express θ(r) through s(r): $\theta(r) = r^{-1} \cdot ds/dr\ (r)$ and write down the series for $\theta = \theta(r)$:

$$\begin{aligned} for\ n = 0: \quad \theta^0(r) &= \theta_0^0 + \theta_1^0 \cdot r + \theta_2^0 \cdot r^2 + \cdots \\ &= \sigma \cdot \left(1 + \frac{1}{2}\alpha\beta\sigma \cdot r^2 + \frac{1}{6}\alpha^2\beta^2\sigma^2 \cdot r^4 + \cdots\right); \\ for\ n = 1: \quad \theta^1(r) &= \theta_0^1 + \theta_1^1 \cdot r + \theta_2^1 \cdot r^2 + \cdots \\ &= \sigma \cdot \left(1 + \frac{1}{4}\alpha\beta\sigma \cdot r^2 + \frac{3}{64}\alpha^2\beta^2\sigma^2 \cdot r^4 + \cdots\right); \end{aligned}$$

$$for\ n=2: \quad \theta^2(r)=\theta_0^2+\theta_1^2\cdot r+\theta_2^2\cdot r^2+\cdots$$
$$=\sigma\cdot\left(1+\frac{1}{6}\alpha\beta\sigma\cdot r^2+\frac{1}{45}\alpha^2\beta^2\sigma^2\cdot r^4+\cdots\right). \quad (17)$$

By induction: odd coefficients $\theta_{2k+1}^{0,1,2}$ are equal to zero; even coefficients $\theta_{2k}^{0,1,2}$ satisfy:

$$\theta_0^{0,1,2}=\sigma; \quad \left|\theta_{2k}^{0,1,2}\right|<\left|\theta_{2k-2}^{0,1,2}\right|\cdot|\alpha\beta\sigma|\ ,\ k=1,2,3,\ldots$$

Taking into account that $0<\mathrm{r}<\mathrm{R_{max}}$, we get an estimate for (17):

$$\theta^{0,1,2}(r)<\sigma\cdot\sum_{k=0}^{\infty}(\alpha\beta\sigma R_{\max}^2)^k.$$

Thus the sufficient condition of uniform convergence for the series (17) with n=0, 1 or 2 is:

$$\left|\alpha\beta\sigma R_{\max}^2\right|<1. \quad (18)$$

If (18) is true, then the function $\theta^{0,1,2}$(r), given by (17), exists; and it is continuously differentiable as many times as we need. It satisfies the boundary condition at r=0. The value of σ is found from the boundary condition at $\mathrm{r}=\mathrm{R_{max}}$: we solve the equation $\theta^{0,1,2}(\mathrm{R_{max}})=\theta^*$ with respect to σ. This equation always has a unique positive solution for any $0\le\theta^*\le 1$. Let us treat $\theta^{0,1,2}(\mathrm{R_{max}})$ as a function of σ. From (17) it is easily seen that this function turns into zero at $\sigma=0$ and grows infinitely and monotonously for $-\infty<\sigma<+\infty$. Therefore it reaches the value $\theta^*>0$ only once for some $\sigma^*>0$, which is the sought solution. Now construction of the series solution $\theta=\theta(\mathrm{r})$ to the system (8)–(11) is completed. As well we can construct the series for $\varphi=\varphi(\mathrm{r})$.

3.2 Analytical solution

We have proved that the system (8)–(11) has a unique classical solution if the condition (18) holds. This result is particularly interesting for the spherical case (n=2), because the analytical solution for n=2 is still unknown [12,13]. Meanwhile we can solve the system (8)–(11) analytically for n=0 and n=1 and compare these solutions with (17). Let $\rho=\mathrm{r}^{n+1}$, then (14) turns into:

$$\rho^{\lambda_n}\frac{d}{d\rho}\left(\frac{ds}{d\rho}\right)=\gamma_n\frac{d}{d\rho}\left(s^2\right),\ where\ \begin{matrix}\lambda_0=0\ and\ \gamma_0=\frac{\alpha\beta}{2}\ for\ n=0;\\ \lambda_1=1\ and\ \gamma_1=\frac{\alpha\beta}{4}\ for\ n=1.\end{matrix} \quad (19)$$

We integrate twice both sides of (19) and then come back to the independent variable r. As a result we obtain:

$$for\ n=0: s(r)=\frac{C_0}{\gamma_0}\cdot tg(C_0 r),\ \ where\ C_0=const>0; \tag{20}$$

$$for\ n=1: s(r)=\frac{C_1 r^2}{1-\gamma_1 C_1 r^2},\ \ where\ C_1=const>0. \tag{21}$$

The solutions to (19) should be continuous, so we get the restrictions on C_0 and C_1:

$$R_{\max}<\frac{\pi}{2C_0};\quad R_{\max}<\frac{1}{\sqrt{\gamma_1 C_1}}. \tag{22}$$

Now we can express the sought functions $\theta=\theta(\mathrm{r})$ and $\phi=\phi(\mathrm{r})$ using (12)–(13):

$$\begin{aligned} for\ n=0\ &: \theta(r)=\frac{C_0^2}{\gamma_0}\cdot\frac{1}{\cos^2(C_0 r)},\quad \varphi(r)=\frac{2}{\alpha}\left(\ln(\cos(C_0 r))+\Phi_0\right);\\ &C_0,\Phi_0=const;\\ for\ n=1\ &: \theta(r)=\frac{2C_1}{(1-\gamma_1 C_1 r^2)^2},\quad \varphi(r)=\frac{2}{\alpha}\left(\ln(1-\gamma_1 C_1 r^2)+\Phi_1\right);\\ &C_1,\Phi_1=const. \end{aligned} \tag{23}$$

Integration constants C_0 and C_1, Φ_0 and Φ_1 may be found from boundary conditions (10)–(11). It is easily seen that (10) is true for any C_0, C_1, Φ_0, Φ_1, while (11) gives us two pairs of equations:

$$for\ n=0: \theta^*\cdot\cos^2(C_0 R_{\max})=\frac{C_0^2}{\gamma_0},\quad \Phi_0=\frac{\alpha}{2}\varphi^*-\ln(\cos(C_0 R_{\max})); \tag{24}$$

$$for\ n=1: \theta^*\cdot\left(1-\gamma_1 C_1 R_{\max}^2\right)^2=2C_1,\quad \Phi_1=\frac{\alpha}{2}\varphi^*-\ln(1-\gamma_1 C_1 R_{\max}^2). \tag{25}$$

The first equation in both pairs (24) is to be solved with respect to C_0 and C_1. We shall prove now that the positive solutions C_0 and C_1 to (24) and (25) always exist, are unique and satisfy (22). Suppose that C_0 runs from 0 to $\pi/2R_{\max}$. Then the left hand side of the first equation of (24) monotonously decreases from θ^* to 0 while the right hand side monotonously increases from 0 to $\pi^2/(2R_{\max})^2\gamma_0>0$. Now suppose that C_1 runs from 0 to $1/\gamma_1(R_{\max})^2$. Then the left hand side of the first equation of (25) monotonously decreases from θ^* to 0 while the right hand side monotonously increases from 0 to $2/\gamma_1(R_{\max})^2 \quad >0$. Due to the features of continuous functions, the graphs of these left and right hand sides will intersect in the considered intervals only once, giving us the sought solutions C_0 and C_1. After that Φ_0 and Φ_1 are explicitly expressed through C_0 and C_1 from the second equations of (24) and (25). The formulas (23) with constants C_0, C_1, Φ_0, Φ_1 from (24) to (25) finally give us the solution to the problem (8)–(11) for n = 0 and n = 1.

Table 1 Power series coefficients for steady state solutions in various coordinate systems

k	Cartesian $s_k(n=0)$	Cylindrical $s_k(n=1)$	Spherical $s_k(n=2)$
0	0	0	0
1	σ	0	0
2	0	$1/2\,\sigma$	0
3	$(\alpha\beta/6)\,\sigma^2$	0	$1/3\,\sigma$
4	0	$(\alpha\beta/16)\,\sigma^2$	0
5	$(\alpha^2\beta^2/30)\,\sigma^3$	0	$(\alpha\beta/30)\,\sigma^2$
6	0	$(\alpha^2\beta^2/128)\,\sigma^3$	0
7	…	0	$(\alpha^2\beta^2/315)\,\sigma^3$

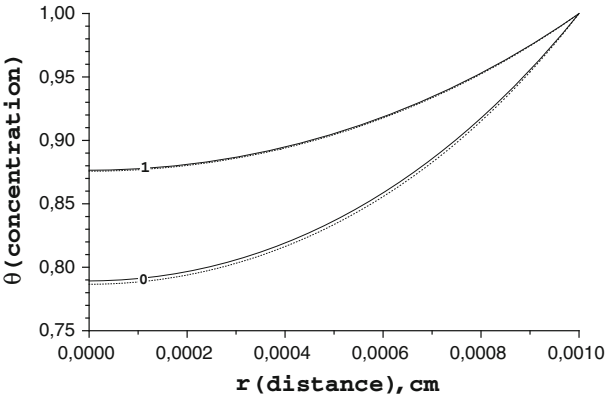

Fig. 1 Steady state solutions: series (*solid line*) and analytical (*dotted line*) in Cartesian (n = 0) and cylindrical (n = 1) coordinates for $\theta^* = 1$

3.3 Comparison of the power series and analytical solutions

We carry out computations with the set of parameters from [10]: $C_{max} = 2.5 \times 10^{-2}$ mol/cm^3, $R_{max} = 10^{-3}$ cm, $\varepsilon = 2.0$, $F = 96{,}485$ coulomb/mol, $R = 8.31$ J/(K mol), $T = 300$ K; $\varphi^* = 1.0$ V, θ^* belongs to [0;1]. Then $\alpha \approx 39$ and $\beta \approx 15{,}156$. We start with comparing the results of paragraphs 3.1 and 3.2: the series solution (17) with coefficients from Table 1 and the analytical solution (23) with constants from (24) to (25) for n = 0 and n = 1. They are shown in Fig. 1. The convergence of the series (17) proves to be good enough: from Fig. 1 it follows that the finite sum with three terms gives us a very good approximation of the exact solution.

Then we compare the series steady state solutions to (8)–(11) with the same parameter values in Cartesian, cylindrical and spherical coordinates. It is easily seen in Fig. 2 that the qualitative shape of these solutions is the same, but for any $0 < r < 1$ we have: $\theta^0(r) < \theta^1(r) < \theta^2(r)$. It means that less ordering of the electrode particles (the clod is less ordered than the fiber and the fiber is less ordered than the film) yields greater final concentrations of intercalated ions.

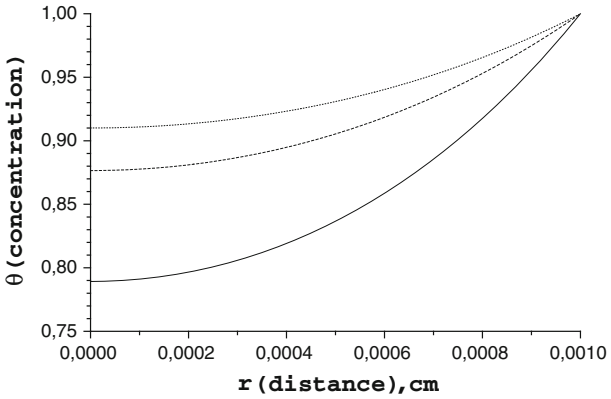

Fig. 2 Series steady state solutions in Cartesian (*solid line*), cylindrical (*broken line*) and spherical (*dotted line*) coordinates

4 Numerical results and discussion

We proceed with the time-dependent solutions to the initial problem (3)–(7). For solving this problem numerically we use the implicit symmetric finite volume difference scheme with the 2-nd order of accuracy:

$$
\begin{aligned}
&\frac{\theta_j^k-\theta_j^{k-1}}{\tau}\\
&\quad=\frac{1}{2h}\frac{D}{(r_j)^n}\left[\left(\frac{r_{j+1}+r_j}{2}\right)^n\cdot\left(\frac{\theta_{j+1}^k-\theta_j^k}{h}+\alpha\cdot\frac{\theta_{j+1}^k+\theta_j^k}{2}\cdot\frac{\varphi_{j+1}^k-\varphi_j^k}{h}\right)\right.\\
&\qquad\left.-\left(\frac{r_{j-1}+r_j}{2}\right)^n\cdot\left(\frac{\theta_j^k-\theta_{j-1}^k}{h}+\alpha\cdot\frac{\theta_j^k+\theta_{j-1}^k}{2}\cdot\frac{\varphi_j^k-\varphi_{j-1}^k}{h}\right)\right];\\
&\theta_0^k=(4\theta_1^k-\theta_2^k)/3;\quad\theta_M^k=\theta^*;\\
&\frac{1}{(r_j)^2}\frac{1}{h}\left[\left(\frac{r_{j+1}+r_j}{2}\right)^n\cdot\frac{\varphi_{j+1}^k-\varphi_j^k}{h}-\left(\frac{r_{j-1}+r_j}{2}\right)^n\cdot\frac{\varphi_j^k-\varphi_{j-1}^k}{h}\right]\\
&\quad=-\beta\left[\theta_j^k+\theta_j^{k-1}\right];\\
&\varphi_0^k=(4\varphi_1^k-\varphi_2^k)/3;\quad\varphi_M^k=\varphi^*;\quad h=\frac{R_{\max}}{M},\quad\tau=\frac{T_{\max}}{N},\quad j=1,\ldots,M-1;\\
&k=0,\ldots,N;\quad n=0,1\ or\ 2.
\end{aligned}
\tag{26}
$$

Here h and τ are the steps with respect to the spatial and temporal coordinates r and t. Being implicit, this scheme is unconditionally stable, and, like the original differential model, this scheme is flux conservative. For solving the nonlinear system of equations on every step we apply the Seidel-type iterations.

The aim of our computational experiment is to compare numerically the influence of the electrode particles' ordering on the Li ion movement in the diffusive layer during intercalation and deintercalation in the absence of the external electric potentials. For this purpose we consider two types of the initial ion distribution: the linear asymmetrical with maximum at the left (inner) or right (outer) boundary and the quadratic symmetrical with maximum in the middle. In both cases we solve (8) with the set of parameters from [10]: $C_{max} = 2.5 \times 10^{-2}$ mol/cm^3, $R_{max} = 10^{-3}$ cm, $T_{max} = 10^2$ s, $\varepsilon = 2.25$, $D = 10^{-6}$ cm^2/s, F = 96, 485 coulomb/mol, R = 8.31 J/(K mol), T = 300 K.

At first we take the initial concentration of ions as $\theta(0, r) = 1 - r/R_{max}$ or $\theta(0, r) = r/R_{max}$, and the initial electric potential as $\varphi(0, r) = \varphi^* = 0$. This kind of the initial data describes the physically relevant situation when the external potential is absent and the electric field appears due to the non-uniform charge distribution. Two variants of θ(0,r) correspond to the two extreme types of ion distribution: they are either concentrate near the particle surface or just emerge at the far boundary of the diffusive layer.

The results are shown in Fig. 3a–c for the Cartesian, cylindrical and spherical models respectively with $\theta(0, r) = 1 - r/R_{max}$. The initial ion concentration and its final steady state distribution are shown with dotted lines; the intermediate results for the time t = 1, 10, 20 and 30 s are shown with solid lines. We see that the qualitative behavior of the solutions to the three models is much the same: the ion concentration slowly evolves to the slightly non-uniform steady state distribution, moving like a wave from the inner (left) boundary r = 0 to the outer (right) boundary $r = R_{max}$. It should be mentioned that in comparison with the slow evolution of the ion concentration θ, the electric potential φ very quickly jumps to its practically constant value. For this reason we do not show the graphs of φ together with the graphs of θ in Fig. 3a–c. Also we do not plot here the numerical results for the initial concentration $\theta(0, r) = r/R_{max}$, because they are quite alike with the described above, with the only difference that the wave goes from right to left.

At the same time there is a distinct difference between the graphs in Fig. 3a–c. The steady state distribution varies significantly: its average amplitude equals 0.5 for the Cartesian, 0.33 for the cylinder and 0.25 for the spherical coordinates. Also for t = 30 s the Cartesian solution is still far from the steady state, while the cylindrical solution practically coincides with it and the difference between the spherical solution and the steady state is less than 10^{-6} already for t = 20 s. It should be emphasized that all these differences appear only due to the different symmetry suppositions, because all other parameters of the three models are exactly the same.

We also solve (8) with the same set of parameters, but with the different initial conditions:

$$\theta(0, r) = \frac{4}{R_{max}^2} r(R_{max} - r); \quad \varphi = \varphi^*. \tag{27}$$

It is done for the proper comparison of the roles of migration and diffusion in the three considered models. The initial conditions (27) are symmetric with respect to r. Pure diffusion would keep this symmetry, but due to the difference of boundary conditions

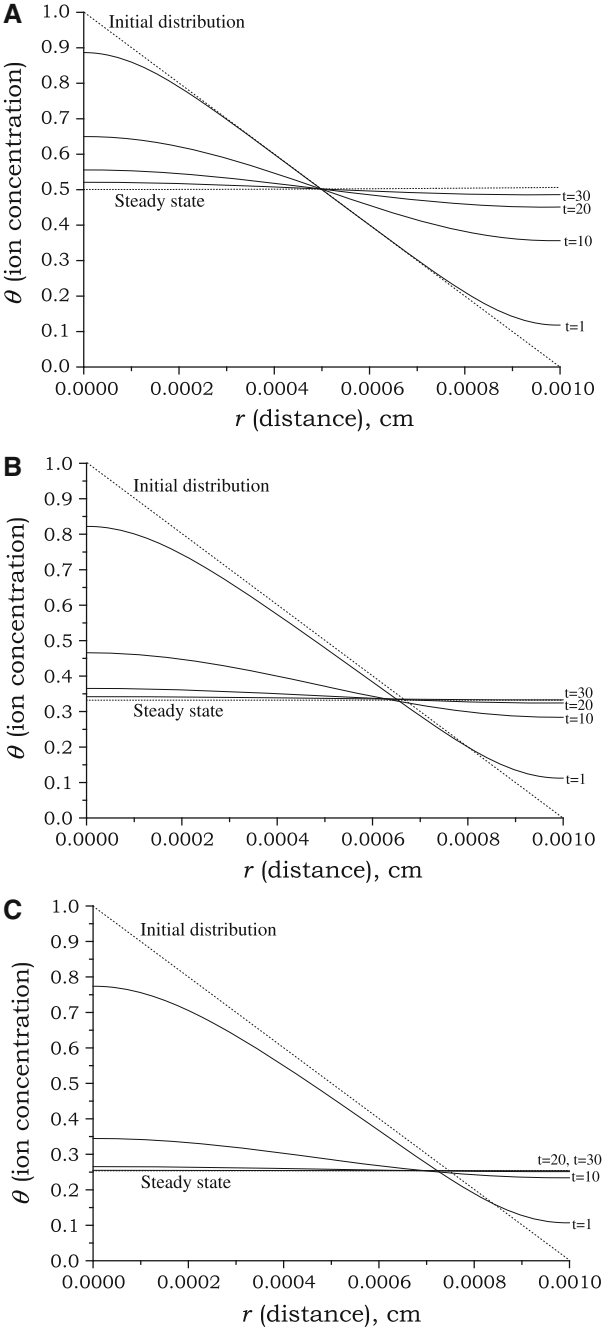

Fig. 3 Ion concentration versus distance from the electrode particle in **a** Cartesian coordinates, **b** cylindrical coordinates, **c** spherical coordinates

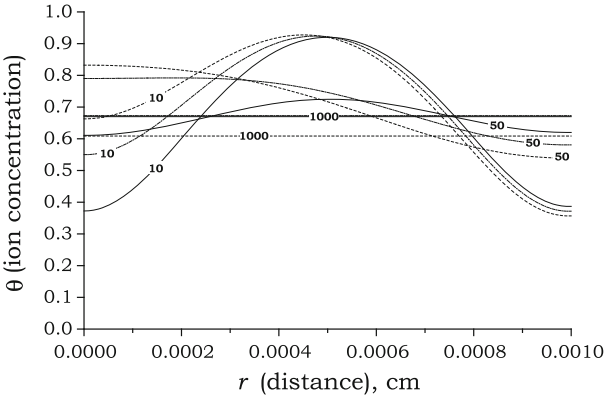

Fig. 4 Ion concentration versus distance from the electrode particle: symmetric initial distribution *solid*, *dash-dotted* and *dotted lines* correspond to Cartesian, cylindrical and spherical coordinates. The labels 10, 50 and 1,000 at the graphs stand for the time in seconds

for ϕ at r = 0 and r = R_{max} the electric field appears; it adds migration to the diffusive motion of ions and breaks the symmetry of the initial distribution, as it is shown in Fig. 4.

It is easily seen that the Cartesian case differs from the cylindrical and spherical: the ion concentration at left (inner) side in the Cartesian model remains lower than at the right (outer) side, while in the cylindrical and spherical models it is vice versa. It is particularly clear at t = 50 s, when the concentration maximum in the cylindrical and spherical models reaches the left side, but in the Cartesian model it remains close to the center. Never the less, the final steady-state distribution in all three cases has the same shape—it is practically uniform with respect to r and has a small increase near the right side. It should be mentioned that the final steady state of the cylindrical model is closer to the Cartesian steady state than to the spherical one, though the evolution of ion concentration in the cylindrical model resembles the spherical evolution much more.

5 Conclusions

We've compared analytically and numerically three models of the ion density and the electric potential distribution around the single charged particle. Very good accuracy of the power series approximate solutions was shown by comparing them with the exact steady state solutions in Cartesian and cylindrical coordinates. Numerically we have demonstrated that various symmetry suppositions (flat, cylindrical and spherical) lead to significant quantitative differences of the steady state solutions, but their shapes are qualitatively similar.

From physical point of view the obtained results may be interpreted as modeling of the processes inside the diffusive layer in the vicinity of the electrode particle. These processes form the environment for the Li+ intercalation at the particle surface. We have demonstrated that the three basic cases of the particle ordering (plane, linear and

chaotic) inside the electrodes of Li-ion batteries exhibit different relaxation time and finally come to the slightly non-uniform steady states with similar shapes, but with different average values.

References

1. M. Doyle, T.F. Fuller, J. Newman, Modeling of Galvanostatic charge and discharge of the lithium/polymer/insertion cell. J. Electrochem. Soc. **140**, 1526–1533 (1993)
2. G. Sikha, R.E. White, B.N. Popov, A mathematical model for a lithium-ion battery/electrochemical capacitor hybrid system. J. Electrochem. Soc. **152**, A1682–A1693 (2005)
3. G.G. Botte, R.E. White, Modeling lithium intercalation in a porous carbon electrode. J. Electrochem. Soc. **148**, A54–A66 (2001)
4. M.W. Verbrugge, P. Liu, Microstructural analysis and mathematical modeling of electric double-layer supercapacitors. J. Electrochem. Soc. **152**, D79–D87 (2005)
5. M.W. Verbrugge, B.J. Koch, Electrochemistry of intercalation materials: charge-transfer reaction and intercalate diffusion in porous electrodes. J. Electrochem. Soc. **146**, 833–839 (1999)
6. Shung-Ik Lee, Yun-Sung Kim, Hai-Soo Chun, Modeling on lithium insertion of porous carbon electrodes. Electrochim. Acta **47**, 1055–1067 (2002)
7. Qi Zhang, Qingzhi Guo, R.E. White, A new kinetic equation for intercalation electrodes. J. Electrochem. Soc. **153**, A301–A309 (2006)
8. Xiaoxia Wang, Koichi Aoki, Transition of current of lithium intercalation from solution to graphite. J. Electroanal. Chem. **604**, 101–108 (2007)
9. Qi Zhang, R.E. White, Comparison of approximate solution methods for the solid phase diffusion equation in a porous electrode model. J. Power Sources **165**, 880–886 (2007)
10. Kandler Smith, Chao-Yang Wang, Solid-state diffusion limitations on pulse operation of a lithium ion cell for hybrid electric vehicles. J. Power Sources **161**, 628–639 (2006)
11. I. Rubinstein, in *Electro-Diffusion of Ions*, SIAM Studies in Applied Mathematics, vol. 11.(SIAM, Philadelphia, 1990)
12. P. Biler, T. Nadzieja, A singular problem in electrolytes theory. Math. Methods Appl. Sci. **20**, 767–782 (1997)
13. A.V. Shobukhov, D.S. Maximov, Mathematical models of symmetrical diffusive layers in porous electrodes. J. Mater. Sci. Eng. A **1**, 592–597 (2011)
14. A. Prohl, M. Schmuck, Convergent discretzations for the Nernst–Planck–Poisson system. Numer. Math. **111**, 591–630 (2009)
15. R.N. Kuzmin, D.S. Maximov, N.P. Savenkova, A.V. Shobukhov, Mathematical modeling of Hysteresis in porous electrodes. J. Math. Chem. **50**, 2471–2477 (2012)